Helmholtz-Zentrum Potsdam
Deutsches GeoForschungsZentrum

Kufner, S.-K., Schurr, B., Sippl, C., Yuan, X., Ratschbacher, L., Akbar, A. s. M., Ischuk, A., Murodkulov, S., Schneider, F. M., Mechie, J., Tilmann, F. (2016): Deep India meets deep Asia: Lithospheric indentation, delamination and break-off under Pamir and Hindu Kush (Central Asia). - Earth and Planetary Science Letters, 435, 171-184.

https://doi.org/10.1016/j.epsl.2015.11.046

Institional Repository GFZpublic: https://gfzpublic.gfz-potsdam.de/

Deep India meets deep Asia: Lithospheric indentation, delamination and break-off under Pamir and Hindu Kush (Central Asia)

Authors:

Sofia-Katerina KUFNER [a,*] (kufner@gfz-potsdam.de)
Bernd SCHURR [a, *] (schurr@gfz-potsdam.de)
Christian SIPPL[a,1] (christian.sippl@anu.edu.au)
Xiaohui YUAN [a] (yuan@gfz-potsdam.de)
Lothar RATSCHBACHER [b] (lothar.ratschbacher@geo.tu-freiberg.de)
Arib s/of Mohammad AKBAR [c] (areeb_201084@yahoo.com)
Anatoly ISCHUK [d] (anatoly.ischuk@gmail.com)
Shohrukh MURODKULOV [d] (shohrukh.m@mail.ru)
Felix SCHNEIDER [a,2] (felix@gfz-potsdam.de)
James MECHIE [a] (jimmy@gfz-potsdam.de)
Frederik TILMANN [a,e] (tilmann@gfz-potsdam.de)

*Correspondence to: kufner@gfz-potsdam.de, schurr@gfz-potsdam.de

Affiliation:

[a] Deutsches GeoForschungsZentrum GFZ, Telegrafenberg, Potsdam, 14473, Germany

[b] Geologie, TU Bergakademie Freiberg, B.-von-Cotta Str. 2, Freiberg, 09599, Germany

[c] Tajik Technical University, Academics Rajabovs Str. 10A, Dushanbe, 734000, Republic of Tajikistan

[d] Tajik Academy of Sciences, 267 Ainy Str., Dushanbe, 734063, Republic of Tajikistan

[e] Geophysik, Freie Universität Berlin, Malteserstr. 74-100, Berlin, 12249, Germany

[1] Present address: Australian National University, 142 Mills Road, Acton ACT, 2601, Australia

[2] Present address: Universität Wien, Althanstr. 14, Vienna, 1090, Austria

Abstract

Subduction of buoyant continental lithosphere is one of the least understood plate-tectonic processes. Yet under the Pamir-Hindu Kush, at the northwestern margin of the India-Asia collision zone, unusual deep earthquakes and seismic velocity anomalies suggest subduction of Asian and Indian lithosphere. Here, we report new precise earthquake hypocenters, detailed tomographic images and earthquake source mechanisms, which allow distinguishing a narrow sliver of Indian lithosphere beneath the deepest Hindu Kush earthquakes and a broad, arcuate slab of Asian lithosphere beneath the Pamir. We suggest that this double subduction zone arises by contrasting modes of convergence under the Pamir and Hindu Kush, imposed by the different mechanical properties of the three types of lithosphere involved. While the buoyant northwestern salient of Cratonic India bulldozes into Cratonic Asia, forcing delamination and rollback of its lithosphere, India's thinned western continental margin separates from Cratonic India and subducts beneath Asia. This torn-off narrow plate sliver forms a prominent high-velocity anomaly down to the mantle transition zone. Our images show that its uppermost section is thinned or already severed and that intermediate depth earthquakes cluster at the neck connecting it to the deeper slab, providing a rare glimpse at the ephemeral process of slab break-off.

Keywords

(1) Pamir-Hindu Kush, (2) India-Asia collision, (3) Slab break-off, (4) Lithosphere delamination, (5) Intermediate depth seismicity, (6) Tomography

1. Introduction

The Pamir and Hindu Kush, located northwest of Tibet, are part of Earth's largest active continental collision (Fig. 1a). As in Tibet, the Pamir-Hindu Kush crust comprises terranes that rifted from Gondwana (the Gondwana terranes of Fig. 1b) and then amalgamated to the southern margin of

 2

Asia (Tapponnier et al., 1981; Burtman and Molnar, 1993; Schwab et al., 2004). Unlike Tibet, the Pamir-Hindu Kush mantle exhibits vigorous intermediate depth (>100 km) seismicity (Billington et al., 1977; Chatelain et al., 1980; Pegler and Das, 1998; Sippl et al., 2013a) (Fig. 1a) and strong velocity anomalies down to the bottom of the transition zone (Koulakov and Sobolev, 2006; Negredo et al., 2007). Fifteen earthquakes with magnitude greater than 7.0 have occurred in the Hindu Kush deep seismic zone in the last 100 years, including the recent destructive October 2015 Mw 7.5 Badakhshan, Afghanistan event (ISC bulletins, 2013; USGS, 2015). Intense intermediate depth seismicity is generally confined to oceanic subduction zones and its occurrence inside a continent is enigmatic (Billington et al., 1977; Vinnik et al., 1977; Chatelain et al., 1980; Roecker, 1982; Burtman and Molnar, 1993; Pegler and Das, 1998). The Pamir and Hindu Kush earthquakes form two separate zones (Fig. 1); the provenance of the Hindu Kush earthquakes is debated (Pegler and Das, 1998; Sippl et al., 2013a), but in the Pamir they are associated with continental Asian plate subduction (Schneider et al., 2013; Sippl et al. 2013b). This contradicts the plate-tectonic paradigm that continental lithosphere does not subduct to significant depth without the pull-force of a leading, negatively buoyant oceanic plate. The understanding of the origin of these anomalies is a key to the deep-seated processes of the India-Asia collision and continental dynamics in general.

We present a regional tomographic model, new earthquake hypocenters and source mechanisms, all based on recent seismic experiments. The detailed lithospheric structure revealed by the tomography and seismicity, and the stress field inferred from earthquake focal mechanisms allow us to deduce the geodynamic processes currently acting under the Pamir and Hindu Kush. We propose a tectonic scenario that led to the unique constellation observed today, suggesting a solution to the long-standing controversy on slab provenance and explaining the formation of the peculiar double subduction zone.

3

2. Data

Our results were obtained from the analysis of seismic data recorded by three temporary networks (Fig. 1a), namely the TIPAGE (Mechie et al., 2012) and FERGHANA (Feld et al., 2015) networks operated between 2008 and 2010 in the Pamir and Tian Shan, and the TIPTIMON network (Schurr et al., 2012; Schurr et al., 2013) from 2012-2014 in the western Pamir, Tajik basin and Hindu Kush. TIPTIMON operated 33 broadband stations in Tajikistan and eight short period sensors in Afghanistan (Mark L-3D, 1 Hz natural frequency) and shared seven sites with the TIPAGE network. The stations in Afghanistan were situated on top of the Hindu Kush intermediate depth seismic zone, allowing to constrain its geometry at high resolution. Additional permanent station data were collected for the operating periods of the temporary networks (Fig. 1b). In total, we analyzed data from 180 seismograph sites with a spacing between ~20 km along a north-south profile in the central Pamir and 40-60 km in the western Pamir, Hindu Kush and Tajik basin. Waveforms from the permanent stations were accessed via the GEOFON, IRIS and Chinese Earthquake Network data centers.

3. Earthquake analysis

3.1 Extended earthquake catalogue

We augmented the existing Pamir-Hindu Kush earthquake catalogue (Sippl et al., 2013a), which is based on the TIPAGE and FERGHANA networks, with the events located during the TIPTIMON experiment between 2013 and 2014, i.e. while the Afghan stations were recording. The superior event-station geometry of this network in relation to the Hindu Kush earthquakes significantly improved their locations. For the earthquake-catalogue production, we followed essentially the same automated procedure applied for the TIPAGE catalogue (see details in Sippl et al., 2013a). Here, we aimed to improve the image of the Hindu Kush seismic zone, therefore only earthquakes that were registered by at least one of the seismic stations in Afghanistan and located west of 71.8°E, the approximate border between the Pamir and Hindu Kush seismic zones, were added to the combined catalogue. To ensure location quality, at least eight P-picks, one S-pick and a root mean square (RMS) residual smaller than one second, based on the initial single event location, were required for event selection. This yielded ~3700 new earthquake hypocenters (Supplementary Fig. 1a, b), which were merged with a subset of the existing event catalogue (Supplementary Fig. 1c). West of 71.8°E, the TIPAGE subset is restricted to events with a maximum backazimuthal gap of 120°, to retain only the best locations under the Hindu Kush. The merged catalogue (Fig. 2) was relocated in a regional 1D velocity model (Sippl et al., 2013a). We applied the double difference location algorithm (*hypoDD;* Waldhauser and Ellsworth, 2000) to improve the relative location of intermediate depth seismicity (for hypocenters deeper than 50 km). This joint relocation not only ensures the consistency of the whole catalogue but also improves the relative locations of individual events with larger backazimuthal gap due to the common recording stations of the different temporal networks.

Absolute location errors were assessed using a probabilistic relocation scheme (*NonLinLoc*; Lomax et al., 2000), where a probability density function (PDF) for the location of each single event is calculated. Commonly, the 68% error ellipse of this PDF serves as a measure for the absolute location uncertainty of the events (Lomax et al., 2000). The average volume of the PDF error ellipses of all events is 270 km^3 (equivalent to a sphere with 4 km radius); the average RMS is 0.31 s. 91 percent of all intermediate depth earthquakes could be relocated with the double difference scheme. The relative location errors of these were obtained by running *hypoDD* in the singular value decomposition mode on subsets of the event clusters, yielding an average relative error of 1.3 km. For those events not relocated with *hypoDD*, mainly isolated events not belonging to a cluster, the single event locations were used.

5

In the updated earthquake catalogue (Fig. 2), the sub-crustal seismicity forms two separate zones: (1) A roughly 90° arc under the Pamir that dips from the Asian side due south in the northeast and due east in the southwest (described in detail by Sippl et al., 2013a); (2) a narrow, slab-like, east-striking and north-dipping structure under the Hindu Kush. In the uppermost mantle, the latter dips clearly north, steepening to sub-vertical at depths greater than ~140 km. Seismicity in this deepest Hindu Kush cluster is very intense, e.g., producing almost one third of all detected intermediate depth earthquakes in our catalogue, despite its compact size.

3.2 Focal mechanisms and stress inversion

We derived earthquake source mechanisms for intermediate depth earthquakes in the time period from 2008 to 2010 in two ways. For 72 events, which were strong enough (M_w 3.9-6.2) to produce sufficient signal at long periods (>10 s), we inverted complete displacement seismograms from all broadband stations in the time domain for the deviatoric moment tensor (Schurr and Nábělek, 1999). All inversions were done interactively to allow quality control of the data and the fit. For 166 events, which were too small for moment tensor inversion, yet had enough coverage in station azimuth and distance range to constrain the two nodal planes, we determined fault-plane solutions from first-motion polarities (Hardebeck and Shearer, 2002). The first motions were picked manually. We kept only earthquakes with more than eight measurements, a maximum azimuthal gap of 150°, and a maximum take-off angle gap of 60° for the focal-mechanism determination. In total, 8200 P-polarities were determined, yielding an average of 49 polarity picks per earthquake. We accepted the best-fit mechanism only if all possible fault-plane solutions had a RMS fault-plane uncertainty smaller than 35° with a maximum of 5% polarity outliers. Maps with event locations, data examples and a comparison of the results obtained from both methods can be found in the Supplementary Material Figure 2.

6

In Figure 3a, we project the tensional (T) axes of the individual source mechanisms on a crooked cross section following the strike of the seismic zones, which is also later used for displaying the tomographic model. Although there is significant scatter, a clear pattern is recognizable. For deep (depth >150 km) events, the T-axes plunge in general steeply but vary slightly between the Hindu Kush and the western and eastern Pamir clusters (Figure 3a). For the central Pamir earthquakes, T-axes plunge more horizontally. The scatter in the stress axes from the individual source mechanisms is expected, because pre-existing weaknesses, probably randomly distributed, allow ruptures to deviate from optimal geometries for the ambient stress field. To estimate the regional stress field, we inverted the fault-plane data for stress tensors (Figs. 3b-f). To satisfy the assumption of a uniform stress field, the mechanisms were subdivided into four sub-regions according to their hypocenter locations and clustering of the T-axis orientations (Fig. 3b). One sub-region encompasses all Hindu Kush earthquakes (52 mechanisms); the other sub-regions follow the Pamir seismicity along strike (western, central and eastern Pamir: 107, 42 and 37 mechanisms). The linear inversion minimizes the total amount of rotation around an arbitrary axis necessary to rotate the focal mechanisms to fit the stress tensor using the software *slick* (Michael, 1987).

To inspect the robustness of the inversion results, we applied a bootstrap test, re-sampling the data set 1000 times and flipping the selected fault and slip directions 10% of the times. Parameters that quantify the quality of the stress tensors are the average rotation angle β and the variance. As the focal mechanisms for the Hindu Kush earthquakes exhibit overall a very similar orientation, the resulting stress tensor is well defined (Fig. 3c), expressed by a low variance (0.104) and a small average rotation angle (24.6°). Re-sampled bootstrap inversions show very stable orientations of the stress axes (σ axes). The mechanisms for the central, western and eastern Pamir (Figs. 3d-f) are more scattered, but all three stress tensors yielded a variance smaller than 0.26. The σ_3 axes confirm the pattern seen in the T-axes ensemble. For the deeper clusters under the Hindu Kush, western and eastern Pamir, they plunge steeply to sub-vertically, while for the shallower central Pamir events σ_3 lies sub-horizontally.

4. Teleseismic tomography

4.1 Travel times

For the regional seismic tomography, we used P-wave travel-time residuals from 1029 teleseismic earthquakes (30-90° epicentral distance, M_w>5.5, Fig. 4a). Earthquake parameters were obtained from the USGS global PDE catalogue. Waveforms were corrected for seismometer response and bandpass filtered between 0.5 and 2.0 Hz. P wave travel times were picked semi-automatically on all available vertical records by detecting the nearest extremum of the waveform to the theoretical onset (Bianchi et al., 2013). We inspected all picks visually and discarded uncertain and noisy ones. In total, 36,339 valid travel-time observations were made, yielding on average 35 picks per earthquake and 200 picks per station. To ensure that events from the two major recording periods were linked, we always required picks from stations that were active during both periods (i.e., re-occupied temporary and permanent stations).

4.2 Tomographic inversion

Our P-wave velocity model was calculated using a modified version of the LOTOS code (Koulakov, 2009), allowing for the inversion of teleseismic data (Bianchi et al., 2013). The inversion for velocity perturbation was performed on a grid with 30 km horizontal and variable vertical node spacing dependent on the ray coverage. To determine the node positions, the ray density was calculated in cubes of 30 km edge length (Fig. 4b). This ray density grid was then scanned along vertical columns, summing up the cumulative ray length, until it exceeded the average ray-length value (here 907 km per cube). Then, a grid node was introduced, the sum was set back to zero and the scanning was continued. This procedure resulted in dense node spacing in well resolved regions

8

and ensured that inversion nodes were only introduced if enough rays were available. The velocity between the nodes is defined by linear interpolation using tetrahedral volumes around the nodes. In the final tomographic model, we only show velocity anomalies that are less than 25 km away from the nearest node, in order not to blur the image by extensive anomalies caused by sparse ray and node density.

Travel-time residuals were calculated from the initial picks including elevation and crustal corrections for each event-station pair separately. For the crustal correction, we constructed a smoothed Moho map based on receiver functions from the TIPAGE, TIPTIMON and FERGHANA deployments (Schneider, 2014) and additional data from the CRUST1x1 model (Laske et al., 2013). The resulting map has a maximum/minimum Moho depth of ~85 /~45 km in the western Pamir and Tajik basin, respectively. The crustal velocities of the background 1D velocity model (ak135; Kennett et al., 1995) were stretched to the depth where the ray penetrates the Moho. Theoretical travel times were then calculated in this modified velocity model. We took the elevations of the recording stations into account by reducing the picked travel times by the theoretical travel time from zero elevation to the station (assuming a P-wave velocity of 5.86 km/s). After applying these corrections, the average residual was subtracted for each event to generate relative travel-time residuals.

The inversion matrix contains elements for the velocity perturbation at each node, elements for station corrections and a regularization block. Station corrections were strongly damped to avoid a trade-off with the shallow mantle structure. The inversion was performed simultaneously for velocity perturbations and station corrections using the LSQR method (Paige and Saunders, 1982). After each iteration, the ray paths and travel-time residuals were recalculated for the updated velocity model. The inversion converged after five iterations. To avoid possible artifacts from grid

9

orientation, we performed the whole inversion procedure on four individual grids, where the x-y coordinate system used for the calculation of ray density and node position was rotated by 0°, 22°, 45° and 67°, respectively (Fig. 4b shows for example the first of these grids). The velocities from these individual inversions were re-sampled on a rectangular grid and then averaged to obtain the final model.

4.3 Evaluation of optimum inversion parameters and checkerboard test

We determined the optimum parameter for flattening by computing synthetic and real models over a set of different flattening values. The optimum parameter yielded the best trade-off between the competing influences of the reduction in RMS travel-time residuals and the increase of model variance (see trade-off curve in Supplementary Fig. 3). The optimum damping parameter and the extent of the well-resolved regions were evaluated from synthetic tests. We calculated theoretical travel times for the resolution tests by 3D ray tracing through a synthetic velocity model using the same station-event geometry as in the real data. Noise was added to the synthetic travel times according to the unmodelled residuals after the inversion of the real data.

Figure 5 shows two sets of checkerboard tests calculated with the optimum flattening parameter (big checkerboard pattern: cubes of 150 km edge length with alternating anomalies of ±3%, separated by a 50 km wide neutral zone; small checkerboard pattern: 100 km anomaly edge length and 25 km wide neutral zone). With our preferred regularization parameters for flattening and damping, amplitude recovery decreased slightly with depth (amplitudes of big checkerboard anomalies at 550 km are ~35% smaller than at 150 km), but the pattern and especially the neutral zone between the anomalies can still be resolved. As expected for teleseismic tomography, vertical smearing exceeds horizontal smearing, and the horizontal extent of the anomalies is accurately mapped in most of the model domains. Only in the deeper layers beneath the western Hindu Kush

10

(~450-600 km, west of ~70°E), the lower ray coverage allows resolution of only the larger checkerboard anomalies. With this set of regularization parameters, the total variance reduction of the travel-time residuals of the real data was 63%. The final station corrections are overall small due to the high damping (extreme values of -0.11 s at station KBU in Kabul/Afghanistan, 0.04 s at EKS2 near Bishkek/Kyrgyzstan and a median of 0.003 s).

4.4 The mantle velocity structure and its relation to the Pamir and Hindu Kush seismic zones

Our three-dimensional teleseismic P-wave model shows a complex high-velocity structure at sub-crustal depths (Fig. 6; see also Supplementary Fig. 4 and Supplementary section 1 for the whole tomographic model, which also includes parts of the Tian Shan). We interpret the relative velocity anomalies as mainly due to temperature differences (Sobolev et al., 1997), i.e., high velocity anomalies (HVAs) likely represent subducted cold lithosphere. Figure 6 displays sections through the tomographic velocity model together with the projected earthquake hypocenters and the σ_3-axes of the stress inversion.

Under the Hindu Kush a strong, narrow high-velocity anomaly reaches from the base of the earthquake zone at ~250 km depth to the bottom of the mantle transition zone at ~600 km depth (anomaly *HK'* in Fig. 6). The Hindu Kush seismic zone itself occurs within neutral velocity material (G_{HK} in Fig. 6). This is in contrast to oceanic subduction zones, where intermediate depth earthquakes occur inside the high-velocity slabs. Slightly displaced southward, adjoining the seismic zone, lies a shallower HVA (*HK)* that connects upwards to the crust and thins from west to east. It is connected to the deeper *HK'* anomaly by a narrow neck of high-velocity material, which appears to be almost severed in the easternmost section through the Hindu Kush (Figs. 6a-c). For the Hindu Kush earthquakes, σ_3 of the stress tensor points vertically down toward the deepest HVA *HK'*, paralleling the sub-vertical dip of the seismic zone and the velocity anomalies, indicating

11

down-dip extension (Fig. 6h). With synthetic tests, we assessed to what extent the neck in the anomaly is resolvable. We built a model with a gap separating the anomalies *HK* and *HK'* as well as one with a continuous HVA between Pamir and Hindu Kush (Figs. 7a, b). Both cases are well resolved, hence, the gap in the HVA containing the Hindu Kush earthquakes and the observed thinning of the anomalies *HK* and *HK'* does not appear to be an artifact. To test the possibility of the presence of a highly thinned lithospheric layer near the Hindu Kush earthquakes, we built a third synthetic model with a 15 km thick high and 15 km thick low velocity layer, simulating a thinned crust-mantle lithosphere compound at the position of the Hindu Kush seismicity (Fig. 7c). Such a thin structure could not be recovered; instead, the extent of the adjacent high-velocity zone is slightly decreased.

In contrast to the Hindu Kush, the deepest Pamir earthquakes coincide with a prominent velocity anomaly (*P* in Fig. 6), crossing the Pamir from the Tarim basin in the east to the Pamir-Hindu Kush syntaxis in the west, where its deepest section *P'* abuts against the deep *HK'* anomaly below ~350 km depth. It overlaps with the Pamir earthquakes in its upper part but penetrates deeper, to ~400 and ~450 km depth in the east and southwest, respectively (Figs. 6d, h). In the center of the Pamir anomaly, a vertical tear (T_P) splits the slab from ~200 to ~400 km depth (Figs. 6f, h). All synthetic models (Fig. 7) show only little vertical smearing at the bottom of the Pamir anomaly, rendering the shape of the slab, the inferred tear and the junction of the Pamir and the Hindu Kush anomalies reliable (*P, P', HK and* T_P in Fig. 6). The σ_3 axes of the Pamir stress tensors vary from dominantly vertically plunging in the western and eastern Pamir to a sub-horizontal orientation in the central Pamir, just above the vertical tear T_P. Hence, the stress field in the Pamir slab appears more complex compared to the Hindu Kush, involving both down-dip stretching at the outer wings of the slab, as well as along-arc stretching and tearing in its curved center (Fig. 6h).

 12

5. Discussion and Interpretation

Combining our observations on lithospheric structure, occurrence of earthquakes, and the intra-slab stress field, we aim to understand the geodynamic processes acting under the Pamir and Hindu Kush. Starting out from this current state, we go back in time to sketch a possible late Cenozoic tectonic history of the western part of the India-Asia collision, which can explain the formation of the major structural characteristics observed today.

5.1 Lithospheric stretching and slab-detachment under the Hindu Kush

In the Hindu Kush, our observation of an inclined upper, downward steepening and thinning HVA, accompanied by increasingly intense seismicity, match numerical simulations of slab detachment following subduction and collision (Duretz et al., 2012; Magni et al., 2012). In these models, shortly before detachment, the slab steepens to near vertical in the deeper part and the subducting lithosphere is highly thinned at the point where the final break-off will happen. Strain localizes where the lithosphere is thinnest. Although the transition between a leading oceanic and subducted continental plate is the preferred zone for slab break-off, subsequent break-offs might occur when continental lithosphere continues to subduct, as has been the case for the Indian plate (Capitanio and Replumaz, 2013). Slab break-off had already been suggested in the Hindu Kush (e.g. Sobolev and Koulakov, 2006; Lister et al., 2008). Here, we confirm this idea and provide clear images of this often postulated but rarely observed tectonic event. Figure 8 shows the synoptic interpretation of our results. The consistent down-dip extensional stress field of the Hindu Kush earthquakes, all the way to the bottom of the crust, indicates that the massive deeper lithospheric fragment (anomaly *HK'*) has to be still attached to its thin, upper continuation (*HK*). This part underlies the inclined upper part of the Hindu Kush seismicity and dips from the Indian side (Figs. 6a-c). The gap between the shallow and the deep HVA (G_{HK}) likely represents the part of the slab where the mantle lithosphere is thinned to an extent that it can no longer be imaged by teleseismic tomography (<30

13

km; see synthetic example in Fig. 7c). The north-dipping Hindu Kush seismic zone is partly separated from the underlying HVA *HK* by a narrow neutral zone (Figs. 6a-c). This offset might mark the resolution limit of our tomography and could arise from a crustal layer (see synthetic test in Fig. 7c), pulled to depth by and still attached to the mantle lithosphere as has been suggested by Roecker (1982). The earthquakes, particularly in the upper inclined section, may actually occur in subducted lower crust, as they do under the Pamir (Schneider et al., 2013). This crustal layer is likely too thin to be resolved by tomography (Sippl et al., 2013b). In a synthetic test, a 15 km thick crustal layer together with a thin remnant lithospheric mantle layer reproduces the observed neutral to slightly reduced velocities (Fig. 7c). The most active seismicity clusters and largest earthquakes both in our catalog (Figs. 2, 6) and global catalogues (e.g., the recent October 2015 Mw 7.5 event, Fig. 6h) occurred adjacent to the thin neck between the *HK* and *HK'* anomalies (Figs. 6a-c) in a depth range between ~180 and 220 km. This agrees well with detachment depths predicted by numerical models for moderate lithospheric ages and convergence rates (e.g., Duretz et al. 2011, 2012). Seismicity is less intense in the western Hindu Kush where the deep and shallow anomalies (*HK* and *HK′*) appear to be still connected (Fig. 6h). This might indicate that the largest earthquakes under the Hindu Kush are directly associated with the final pinching-off (Lister et al., 2008). We might in fact witness the point in time, where the Hindu Kush slab is just about to break free. Although viscous necking is likely to be the dominant deformation mechanism (Duretz et al., 2012), strain localization may produce such high strain rates that brittle failure is enabled.

Assuming that the Hindu Kush anomalies once formed an intact lithospheric slab, the thinning and necking of the upper part of the Hindu Kush slab implies that the initial length of subducted lithosphere was less than its current penetration depth. Thus, the total length of the lithosphere has to be corrected for stretching in any paleogeographic reconstruction. We estimated the first-order magnitude of this extension under simplified assumptions. The Hindu Kush slab is significantly

14

thinned in its upper part between ~50 and 300 km depth. Here, it is on average less than 50 km thick, compared to a thickness of ~150 km below ~300 km depth. This amounts to ~66% thinning assuming plane strain (schematically shown in Fig. 9a). Restoration would hence shorten the upper 250 km of the slab to ~83 km length. Between 250 and 300 km, the slab is already that thin, that it can be neglected. The total slab penetration is ~600 km (Fig. 6; Koulakov and Sobolev, 2006; Negredo et al., 2007) and the total restored slab length is hence ~380 km (Fig. 9b). Subducting ~380 km of slab at ~34 mm/yr (Molnar and Stock, 2009) takes ~11 Myr, suggesting that the Hindu Kush slab is a young feature in the India-Asia collision history. Obviously, this is a rough estimate, as slab-thickness measurements are affected by uncertainties in the tomographic model, although the lateral resolution is very good in this region (Fig. 7). The lower portion of the Hindu Kush slab could have been shortened, which would lead to an overestimation of its original thickness. The Pamir anomaly, which penetrates to ~400 km depth, is apparently less affected by vertical stretching, as no significant thinning of the HVAs *P* and *P'* is observed (Fig. 6d). Thus, the restored Hindu Kush slab (Fig. 9b) and the Pamir slab (Fig. 6d) appear to have a similar length.

5.2 Slab provenance – one or two plates?

The complex topology of the seismic planes under the Pamir and Hindu Kush has puzzled scientists for a long time. Interpretations ranged from the juxtaposition of two subduction zones of opposite polarity (Chatelain et al., 1980; Burtman and Molnar, 1993; Negredo et al., 2007) to one-plate models either of Indian (Billington et al., 1977; Pegler and Das, 1998) or Asian provenance (Sippl et al., 2013a). Our new data together with other recent results help to clarify the situation. The Hindu Kush earthquake zone outlines a structure that dips moderately, but clearly to the north between the Moho at ~60 km depth and ~140 km depth (Figs. 2, 6a-c). This is in agreement with the observations of Pegler and Das (1998), who inferred an Indian origin of the Hindu Kush slab based on the dip of the earthquake zone. That the north-dipping seismic zone is underlain by high

15

velocity material on its southern side (Fig. 6a-c) strongly supports this interpretation. Any other configuration, e.g., a contorted and overturned slab of Asian origin would not comply with this geometric relation. Consequently, we infer that the Hindu Kush mantle anomalies belong to lithosphere that came from the south, from the Indian side.

Compared to the Hindu Kush, the Pamir velocity anomalies are bent and offset northwards (Fig. 6), just as the Pamir seismic zone (Fig. 2) and tectonic structures (Fig. 1). Recent geophysical studies related the Pamir seismic zone (Sippl et al., 2013a) and associated mantle anomalies to depths of ~180 km to subduction of Asian lithosphere (Sippl et al., 2013b, Schneider et al., 2013). The deeper Pamir velocity anomalies imaged here (Figs. 6d, e) likely represent the continuation of the same down-going Asian plate, as it overlaps in the upper part with the structures imaged by Sippl et al. (2013b) and Schneider et al. (2013). Together with our inference on the provenance of the Hindu Kush slab, the currently available observations strongly suggest a two-plate model, where the Hindu Kush slab is subducting from the Indian side, detaching and abutting against the western edge of the arcuate Asian Pamir slab at depth. This configuration is sketched in Figure 8.

5.3 A scenario for the recent tectonic history of the western India-Asia collision

The problem remains how the peculiar configuration of two narrow plates of different continental origin subducting next to each other in opposite directions formed. While the Hindu Kush slab is straightforwardly explained as part of the subduction of the Indian slab, the retro-side subduction and along-arc stretching and tearing of the Asian Pamir slab is more difficult to explain. We suggest that the peculiar configuration of two slabs of different tectonic origin (Fig. 8) arises quite naturally when considering the shape, structure and rheology of India and Asia during the collision history. Paleomagnetic reconstructions, geological balancing, and global tomography (Van der Voo et al., 1999; Guillot et al., 2003; van Hinsbergen et al., 2011) demand that before the Indian cratonic

16

lithosphere (*Cratonic India* in Fig. 10) arrived at the Asian margin, some 1000 km of a (super-)extended passive margin, so-called Greater India, was subducted. Cratonic India's buoyancy, with its thick and stable Proterozoic crust and depleted mantle lid (Kumar et al., 2001), presumably choked the subduction zone, leading to the break-off of the Greater Indian slab (DeCelles et al., 2002; Stearns et al., 2013, 2015). Its remains are apparently resting now just below the mantle transition zone (Van der Voo et al., 1999; Replumaz et al., 2010; Capitanio and Replumaz 2013; schematically sketched in the inset of Fig. 10a). After break-off of Greater India, the mode of convergence switched from subduction to underthrusting. Underthrusting of India might have been facilitated by the constitution of Asia's southern margin at the time. It was built by the amalgamated Gondwana terranes that form the Pamir, Karakoram and Tibet crust today (Guillot et al., 2003; Schwab et al., 2004). The lithosphere of these terranes was rheologically weakened by a long history of subduction, accretion, arc formation and tectonism (e.g., Schwab et al., 2004; Schmidt et al., 2011; Smit et al., 2014; Stearns et al., 2015). Although Asian and Indian rocks now abut along the Indus-Yarlung suture at the surface (Fig. 1), Indian mantle lithosphere and possibly lower crust underthrusted Asia several hundred kilometers further north (Nábělek et al., 2009, Kind and Yuan, 2010), reaching the Tarim basin in westernmost Tibet (Li et al., 2008) and also underthrusting the Pamir (Mechie et al., 2012; Sippl et al., 2013b). We suggest that the Tarim-Tajik cratonic lithosphere (*Cratonic Asia* in Fig. 10) constituted the first real obstacle for advancing Cratonic India as the Gondwana terrane collage further to the south likely lacked a lithospheric keel (e.g., Schwab et al., 2004; Schmidt et al., 2011; Smit et al., 2014; Stearns et al., 2015). Then, the first contact between Cratonic Asia and Cratonic India must naturally have occurred along India's western promontory. Its imprint is still visible in topography and structural grain from the western Himalaya to the northern Pamir (Fig. 1). As the two cratons started to collide here, it must have had consequences for the style of deformation.

We estimated that the central portion of the Pamir slab and the restored Hindu Kush slab have roughly a similar length (Section 6.1, Fig. 9). Rolling back the collision by this amount places the underthrusted Indian lithospheric spur along the straight line connection between today's southern Tajik basin and southern Tarim basin (Fig. 10a). We suggest that this was the southern margin of Cratonic Asia, which got subsequently indented, forcing the Asian lithosphere to roll-back and forming the Pamir slab (Fig. 10b).

India's western salient is delimited on its western flank by a deformed margin, which terminates at the present plate boundary along the Chaman fault system (Fig. 1b). The structure of this margin is well exposed in Pakistan's Katawaz basin (Fig. 1b), where strongly folded marine sediments overlie a thin transitional basement (Tapponnier et al., 1981; Treloar and Izatt, 1993; Mitra et al., 2006). It probably constitutes a vestige of India's extended continental margin (Replumaz et al., 2010), akin in structure and rheology to the vanished Greater India. Extrapolating India's now underthrusted western margin to the north, it naturally connects to the Hindu Kush earthquake zone (Fig. 1). We consequently propose that the narrow slab that subducts under the Hindu Kush is India's extended western continental margin (*Marginal India* in Fig. 10). Convergence between India and Asia must have been accommodated differently for Cratonic and Marginal India due to their difference in buoyancy. While Cratonic India's buoyant spur penetrated into Cratonic Asia, Marginal India's thinner crust and denser lithosphere separated from Cratonic India and subducted beneath Cratonic Asia. At this point (at ~10 Ma), the Pamir crust, which was pushed onto Cratonic Asia (the former connection of the Tajik and Tarim basins), was already critically thickened (Schmidt et al., 2011; Stübner et al., 2013; Smit et al., 2014, Stearns et al., 2013, 2015). Its load depressed the Asian lithosphere, initiating its subduction. Hence, to the extent that Cratonic India advanced into Asia and forced the Asian lithosphere to roll back under the Pamir, Marginal India subducted under the Hindu Kush, forming the two oppositely dipping slabs (Fig. 10b). The process of pushing back and bringing down the Asian plate is thus more akin to delamination than classic plate subduction, driven initially not primarily by gravitational instability but by the penetration of India. Rollback of the Pamir slab must have caused along-arc extension, recorded by the more shallow Pamir earthquake mechanisms (Fig. 6h). As the Pamir slab was forced to retreat in its center and was bent around the western corner of advancing Cratonic India, it tore apart in the middle (Fig. 8). If the Pamir slab became partly eclogitized (Sippl et al., 2013b), negative buoyancy would accelerate the roll-back and tearing.

6. Conclusion

The Pamir and Hindu Kush are the only place in the India-Asia collision zone where deep earthquakes occur, strong velocity anomalies penetrate deeply into the mantle and continental crust subducts to at least 150 km depth without the help of a leading oceanic plate. We evaluated seismic data from recent temporary deployments in the Pamir and Hindu Kush in order to understand why this happens. Using detailed seismicity, earthquake source mechanisms and stress inversions, and high-resolution tomographic images, we show that the Hindu Kush earthquakes are caused by the detachment of a foundering lithospheric plate sliver that once was India's continental margin. In contrast, the velocity anomaly under the Pamir is caused by Asian lithosphere (Cratonic Asia), which is forced to delaminate and roll back by the northward advancing promontory of Indian lithosphere (Cratonic India). While buoyant Cratonic India bulldozes into Cratonic Asia, the heavier Marginal India lithosphere tears off from Cratonic India and subducts. Hence, the different mechanical properties of the adjacent lithospheres (Marginal India versus Cratonic India) activated the two contrasting modes of convergence, side by side and coevally under Pamir and Hindu Kush, forming the two juxtaposed subduction zones observed today.

Acknowledgements This research is part of the CAME project bundle TIPTIMON, funded by the

19

German Federal Ministry of Education and Research (support code 03G0809), and the DFG bundle TIPAGE (PAK 443). The Geophysical Instrument Pool Potsdam (GIPP) provided seismic instruments for the temporary networks. Data from the temporary networks (FDSN codes: 7B 2008-2010; 6C 2009-2010 and 2013-2014 (Schurr et al., 2013); 4B 2008-2009; 5C 2012-2014 (Schurr et al., 2012)) are archived at GEOFON data center, permanent station waveform data can be obtained through the IRIS DMC (KN – 10 stations used here, KR-13 (Institute of Seismology, National Academy of Sciences of Kyrgyz Republic (KIS), 2007), KZ-4 (KNDC/Institute of Geophysical Research (Kazakhstan), 1994), TJ-7 (PMP International (Tajikistan), 2005), II-3 (Scripps Institution of Oceanography, 1986), IU-1 (Albuquerque Seismological Laboratory (ASL)/USGS (1988)), GEOFON (CK-4, GE-1 (GEOFON data centre, 1993), KC-2 (CAIAG Central Asian Institute for Applied Geosciences, 2008)) and the Chinese Earthquake Network data centers (9 stations). Focus Humanitarian Assistance and Afghanistan Geological Survey organized the seismometer deployment in Afghanistan. The TIPAGE and TIPTIMON groups at GFZ Potsdam and TU Bergakademie Freiberg, and M. Bianchi and C. Haberland contributed fieldwork, technical support and discussions. S. Heimann helped with his pyrocko software with the projection of the stress axes (Krieger and Heimann, 2012). M. Dziggel helped in preparation of the schematic figures.

 20

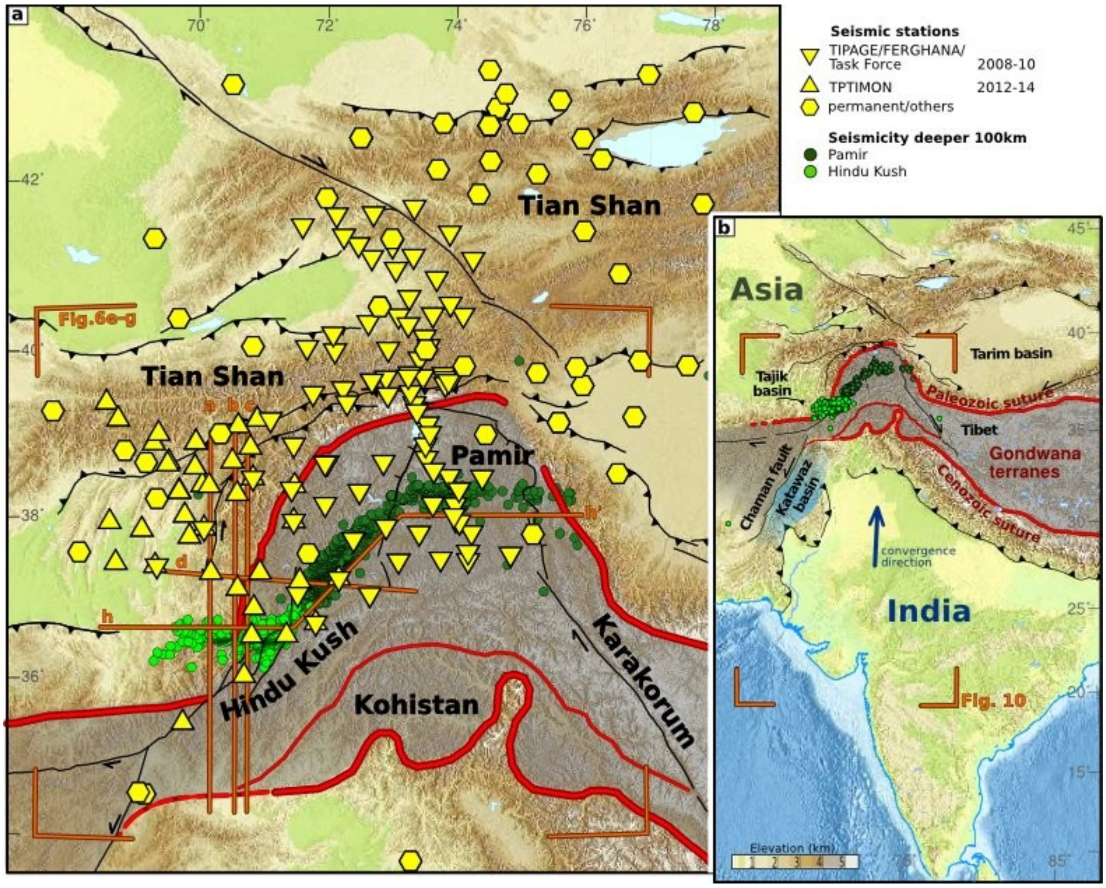

Figure 1: **Seismicity and seismic station used in this study plotted onto a topographic map of Central Asia.** (**a**) Yellow symbols mark seismic stations. Northern red line follows the Late Paleozoic-Triassic suture separating cratonic Asia in the north from the Gondwana terranes (shaded grey) in the south. Southern line is the Cenozoic Indus-Yarlung suture, separating Indian from Asian rocks. Thin red line marks the Shyok suture. Seismicity (Sippl et al., 2013a) for depths greater than 100 km is plotted in light and dark green under the Hindu Kush and Pamir, respectively. Orange markers locate the sections in Figure 6. (**b)** India and its collision with Asia. Deep (>100 km) seismicity for the last 50 years from a global catalogue (Engdahl et al. 1998).

 21

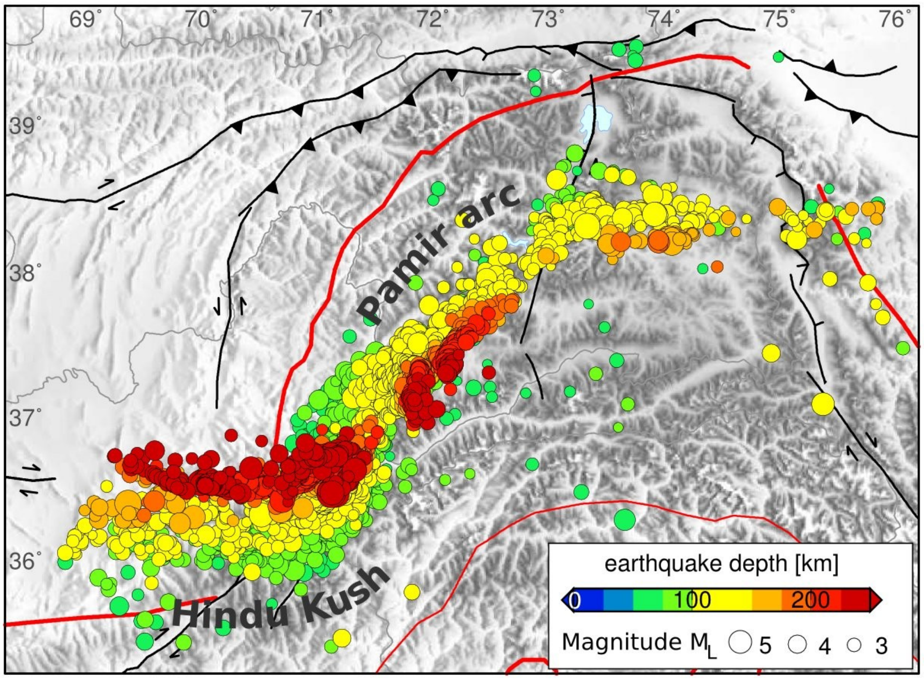

Figure 2: Updated earthquake catalogue for the Pamir and Hindu Kush. Earthquake catalogue at sub-crustal depths with hypocenters deeper than 50 km. Size of the symbols corresponds to local magnitude, color to depth. Hypocenters are sorted by depth where deepest earthquakes are plotted on top. Main tectonic features as in Figure 1a.

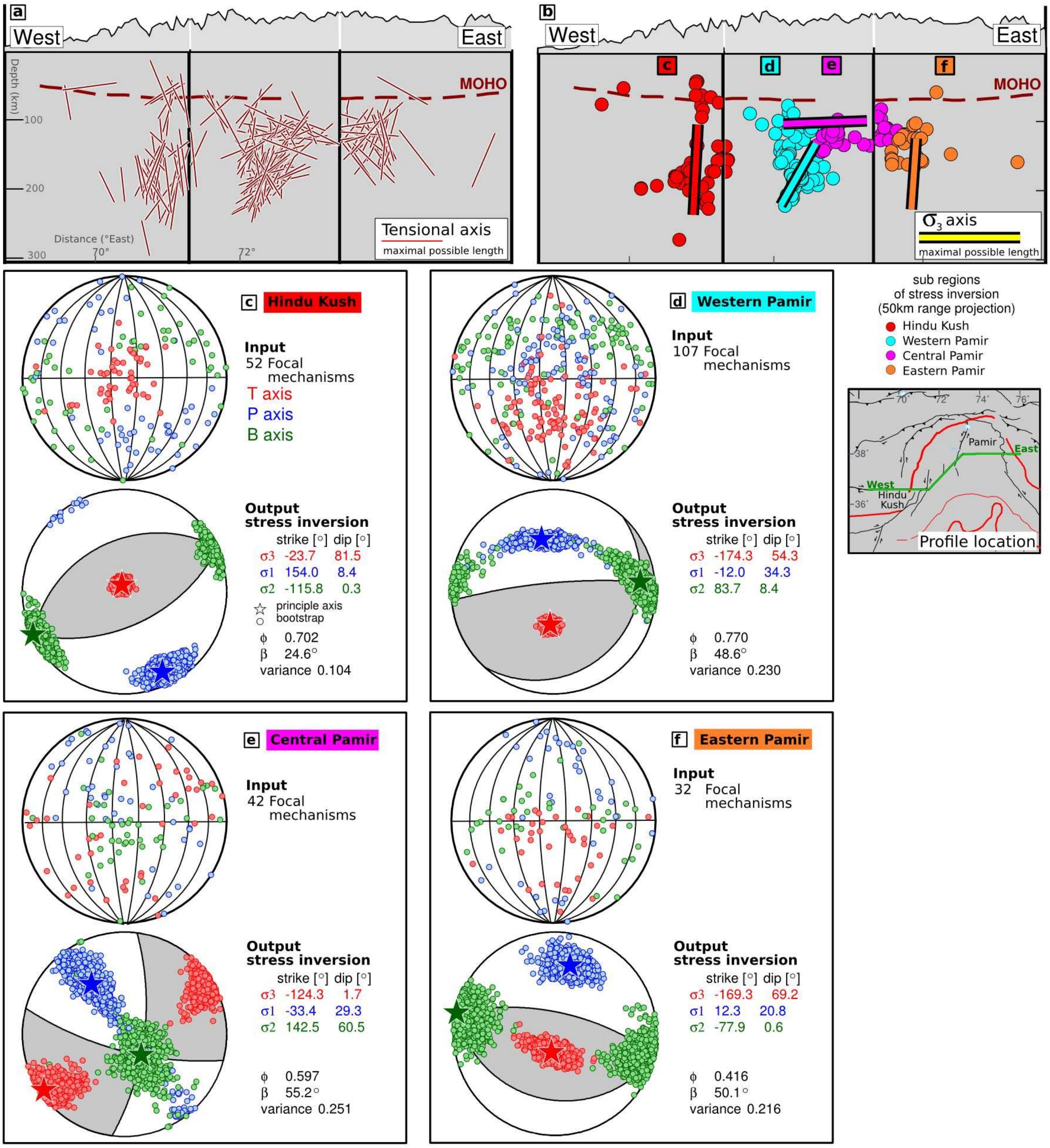

Figure 3: Earthquake tensional axes and stress inversion. (a) σ_3 axes (T-axes) from 238 earthquake focal mechanisms projected onto cross section of Figure 6h. Length of vectors scales with in-plane proportion of their amplitudes (longest possible vector is 100% in-plane, point means perpendicular to plane). (**b**) Partitioning of earthquakes in four sub-regions (color coded) for the stress inversions and resulting σ_3 axes projections. (**c-f**) Top panels: Principal axes of focal mechanisms in a stereonet used as input to the stress inversion. Bottom panels: Inverted stress tensors plotted as beachball and with principal stress axes (stars). $\Phi=(\sigma_2-\sigma_1)/(\sigma_3-\sigma_1)$ is the relative stress magnitude, β the average rotation angle. Colored circles indicate results of bootstrap inversions, providing a measure of inversion robustness.

 23

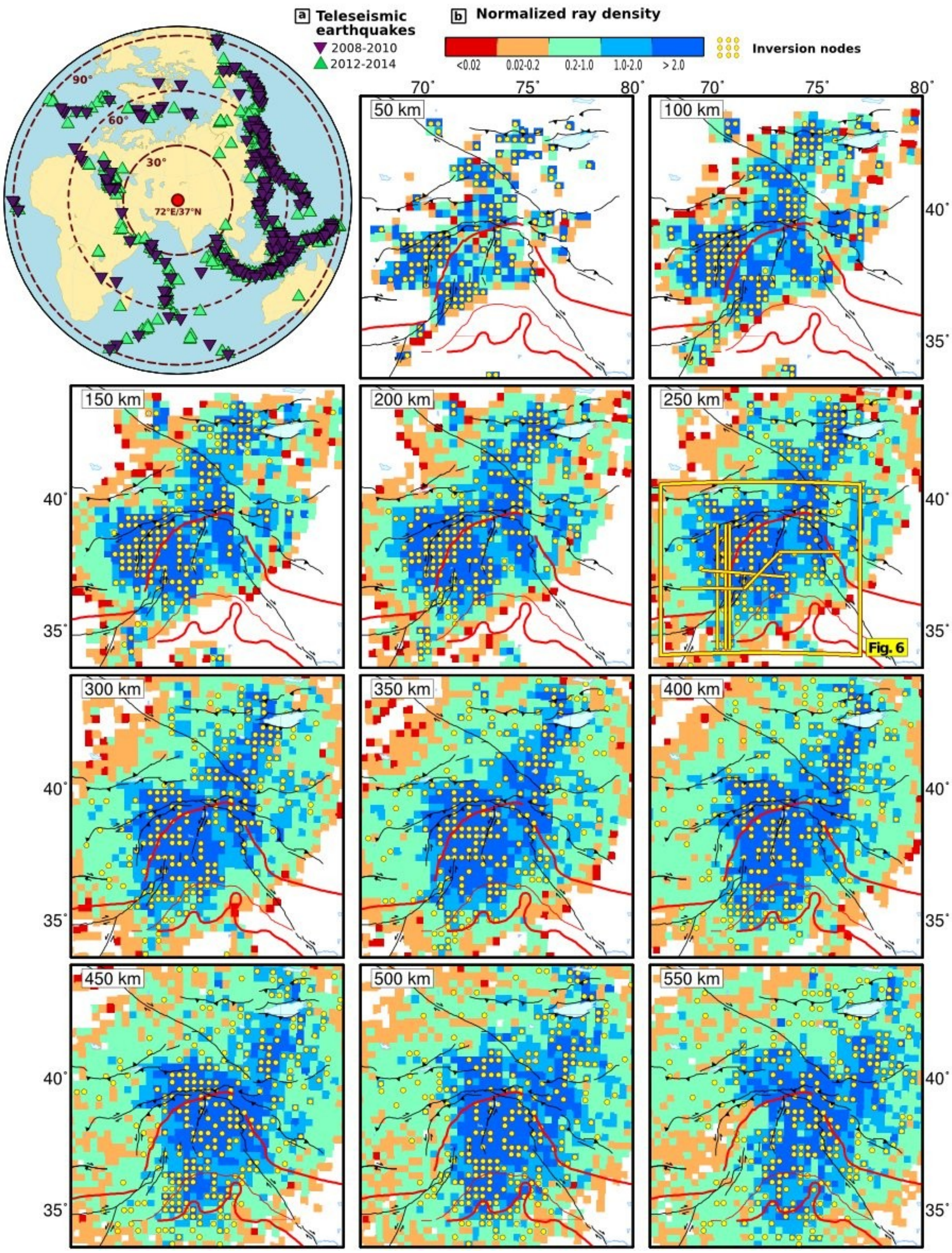

Figure 4: Distribution of teleseismic earthquakes and ray coverage. (a) Location of teleseismic earthquakes used in tomography. Colors differentiate the two recording periods. (**b**) Ray coverage: cumulative ray length in each 30 km cube, normalized by the average length per cube. Yellow dots mark the node positions in the inversion grid (vertical projection width: ±25 km). The positions of the cross sections shown in Figure 6 are plotted for orientation in the 250 km slice. Main tectonic features as in Figure 1a.

503

24

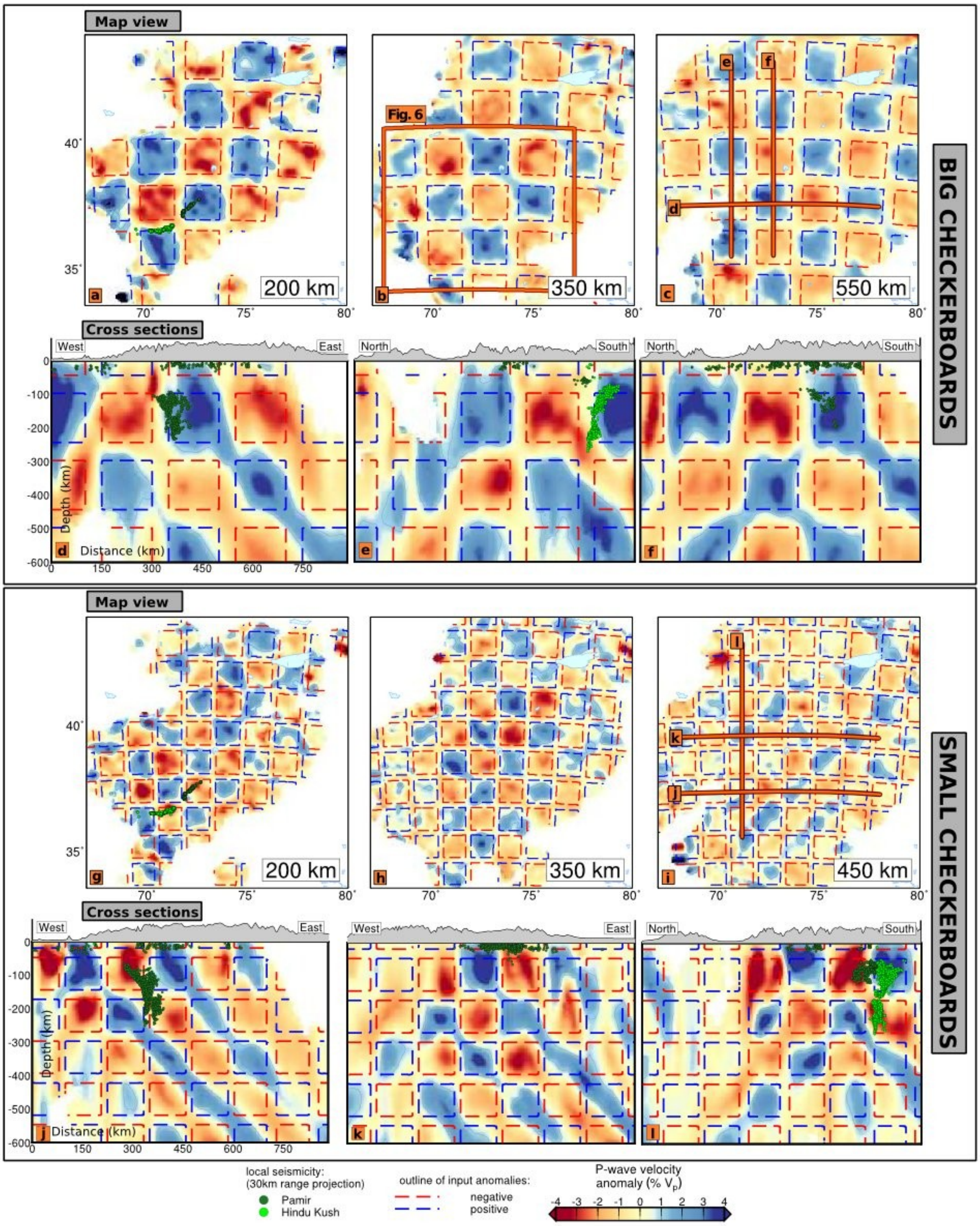

Figure 5: Checkerboard tests. The recovered output velocity model is color coded as in Figure 6. Seismicity from Figure 2 is plotted for orientation. **(a-f)** Input anomalies (dashed, ±3%) are cubes of 150 km edge length separated by a 50 km wide neutral zone. **(g-l)** Cubes with edge length of 100 km separated by 25 km wide neutral zone.

25

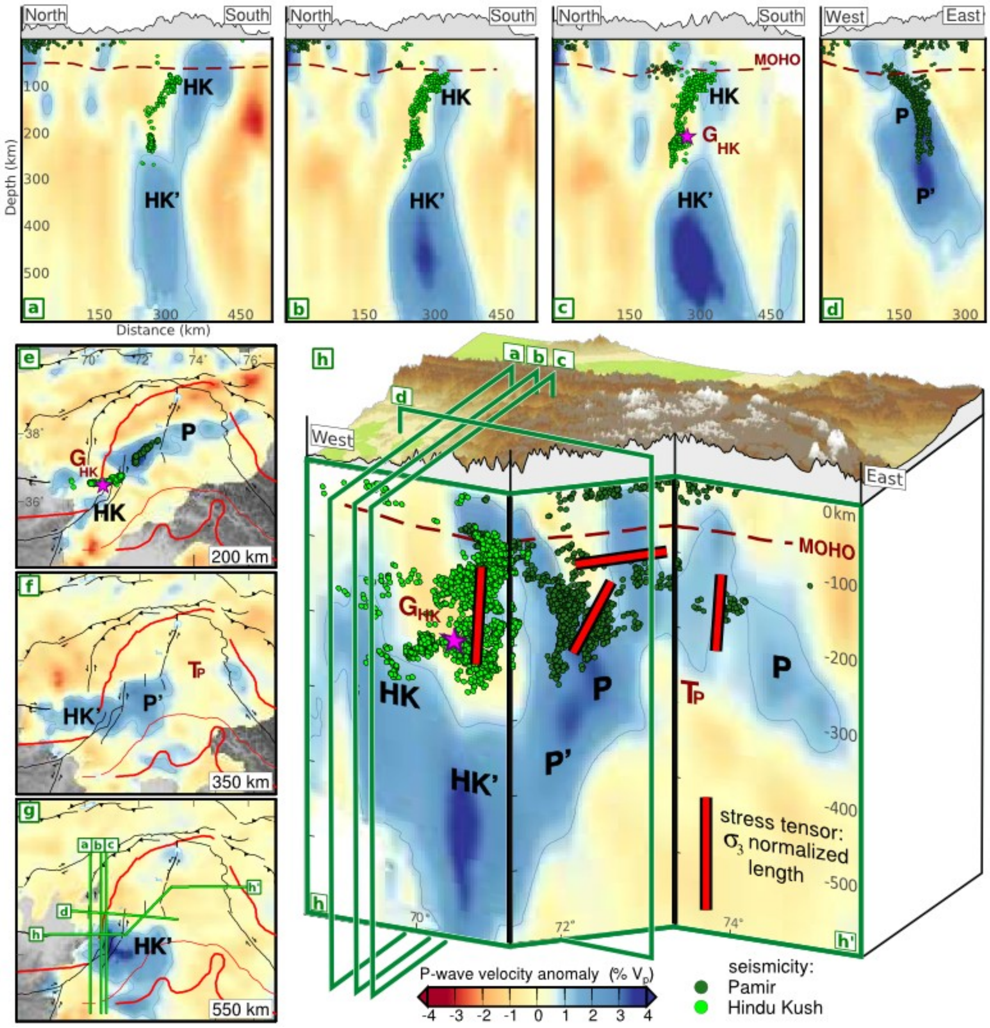

Figure 6: Tomographic velocity model, seismicity and stress axes. (**a-d)** Vertical sections. (**e-g)** Depth maps. (**h)** Vertical section along the Hindu Kush and Pamir slabs (+1% anomaly of the velocity model is contoured). Earthquakes of the Pamir (dark green) and Hindu Kush (light green) seismic zones (30 km swath width) and σ_3 (tension) axes (red bars) from stress inversions of 238 focal mechanisms projected onto the cross-section planes. Capital letters mark anomalies described in the text. Pink star marks the hypocenter of the recent October 2015 Mw 7.5 Badakhshan, Afghanistan event (USGS, 2015). Discrepancy between USGS event locations and our catalogue is less than 10 km at this depth.

26

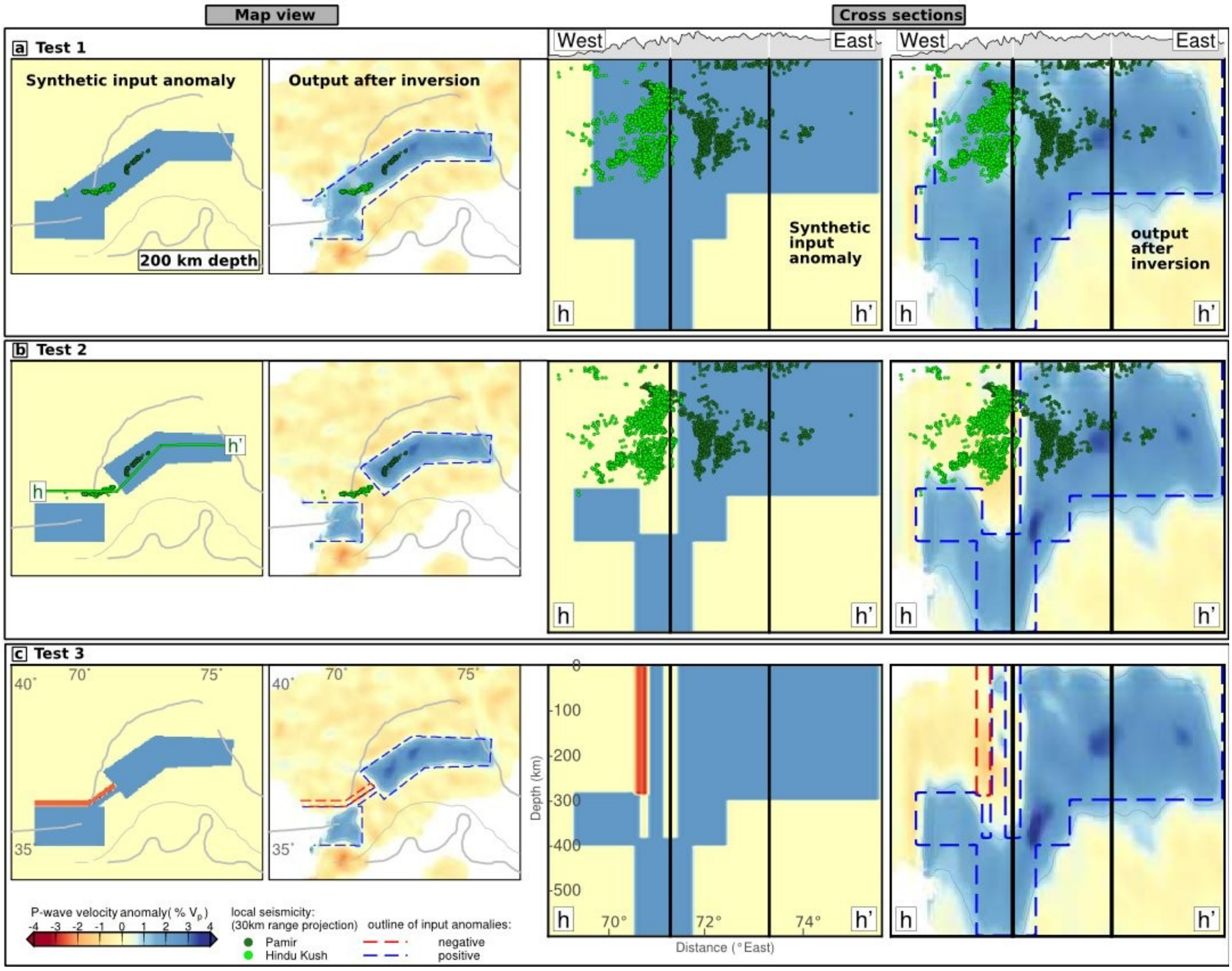

Figure 7: Synthetic tests to assess the reliability of the features discussed in the text. Left panels show the input synthetic anomalies, right panels the recovered models (input anomalies dashed). Map view and cross-section as in Figures 6e, h. Earthquakes and tectonic features as in Figure 6. **(a)** Scenario 1: Pamir-Hindu Kush anomalies are connected in the upper mantle. (**b**) Scenario 2: Pamir-Hindu Kush anomalies are separated in the upper mantle and the Hindu Kush earthquakes occur in the gap. (**c**) Scenario 3: A ~15 km thick low and a ~15 km thick high velocity zone occupy the zone between the Pamir and Hindu Kush anomalies.

505

27

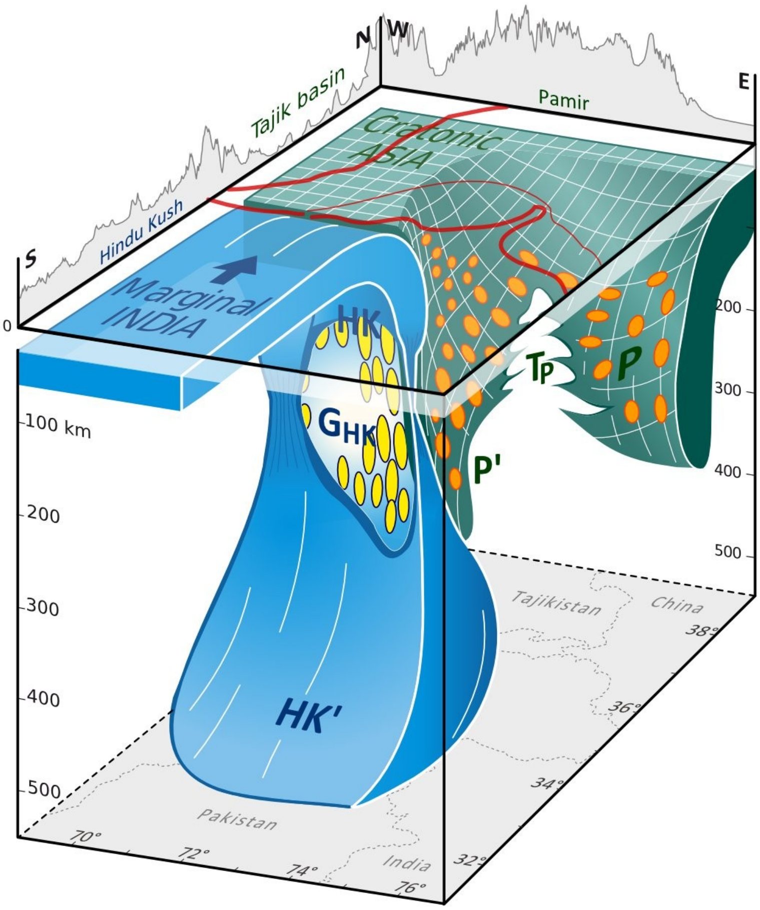

Figure 8: Synoptic interpretation of the tomographic model. Blue: The Indian-plate sliver detaching under the Hindu Kush. Earthquakes (yellow) cluster in regions of stretching and necking where lithosphere is extremely thinned. Green: Asian plate delamination and rollback under the Pamir, with along-arc stretching and central tearing; Pamir earthquakes in orange. Capital letters mark the velocity anomalies described in the text and annotated in Figure 6.

506

28

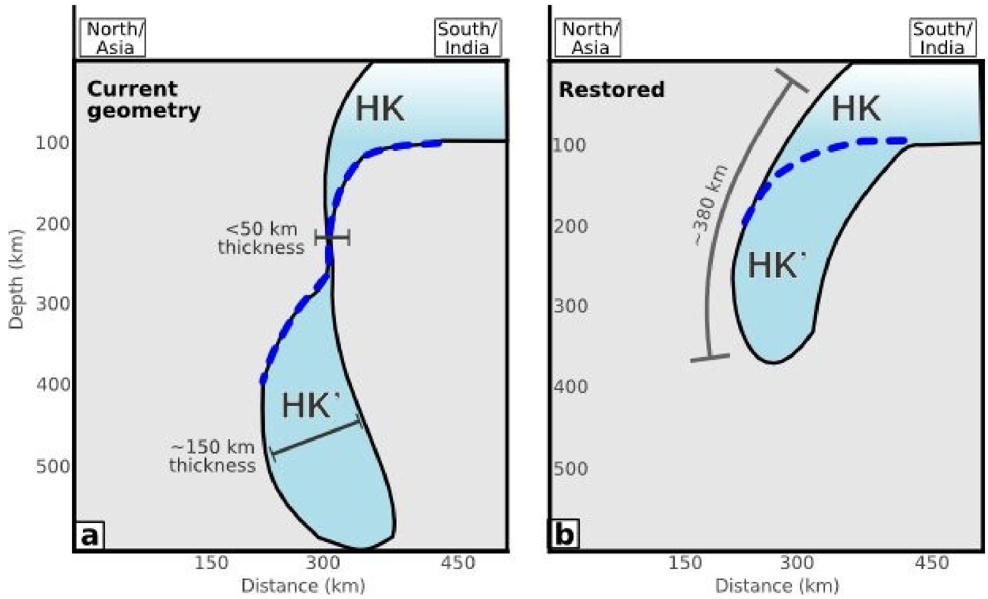

Figure 9: Sketch of slab-restoration for the Hindu Kush. (a) Current situation similar to imaged Hindu Kush slab (Figs. 6a-c). (**b**) Restored slab. Although addressing the mechanism of slab stretching is beyond the scope of this article, current geometry may have been achieved by simple shear extension as sketched; the final detachment is probably due to necking.

507

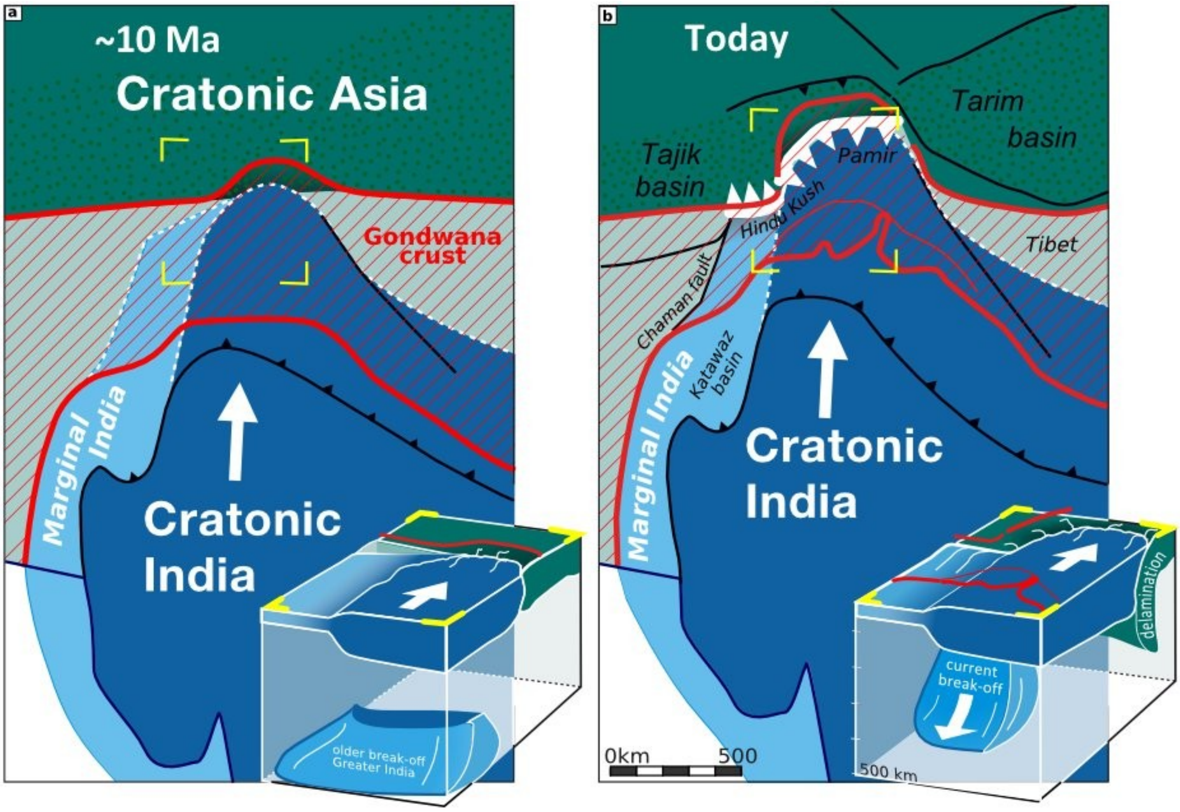

Fig. 10: Evolution scenario of the western India-Asia collision zone for the ~10 Myr of collision history. Sketches outline the tectonic plates at depth, which differ from the boundaries at the surface (sutures as in Fig. 1). Insets focus on the Pamir-Hindu Kush, illustrating the plate interaction in perspective view (region and view point as in Fig. 8) (**a)** At ~10 Ma, the Indian cratonic lithosphere (Cratonic India) impinges on Asian cratonic lithosphere (Cratonic Asia, comprising the basement of the Tarim and Tajik basins), pushing thickened crust, comprising rheological weak Gondwana crust (hatched red) on top. The previously subducted Greater Indian lithosphere (extended passive margin of India) has already detached along the entire collision front, allowing a rearrangement of the continental subduction system. (**b**) Present: Cratonic India has underthrusted the Pamir, shortened the Gondwana crust, and indented Cratonic Asia, which delaminates and rolls back. The thinned and less buoyant crust of the western passive margin of India (Marginal India) tears off from Cratonic India and subducts under Asia.

508

References:

Albuquerque Seismological Laboratory (ASL)/USGS, 1988, Global Seismograph Network (GSN - IRIS/USGS). International Federation of Digital Seismograph Networks. Other/Seismic Network. doi:10.7914/SN/IU.

Bianchi, M., Heit, B., Jakovlev, A., Yuan, X., Kay, S. M., Sandvol, E., Alonso, R. N., Coira, B., Brown, L., Kind, R., & Comte, D., 2013. Teleseismic tomography of the southern Puna plateau in Argentina and adjacent regions. *Tectonophysics*, *586*, 65-83.

Billington, S., Isacks, B. L., & Barazangi, M., 1977. Spatial distribution and focal mechanisms of mantle earthquakes in the Hindu Kush–Pamir region: A contorted Benioff zone. *Geology*, *5*(11), 699-704.

Burtman, V. S., & Molnar, P., 1993. Geological and geophysical evidence for deep subduction of continental crust beneath the Pamir. *Geological Society of America Special Papers*, *281*, 1-76.

CAIAG Central Asian Institute for Applied Geosciences, 2008. Central Asian Seismic Network of CAIAG. International Federation of Digital Seismograph Networks. Other/Seismic Network. doi:10.7914/SN/KC.

Capitanio, F. A., & Replumaz, A., 2013. Subduction and slab breakoff controls on Asian indentation tectonics and Himalayan western syntaxis formation. *Geochemistry, Geophysics, Geosystems, 14*(9), 3515-3531.

Chatelain, J. L., Roecker, S. W., Hatzfeld, D., & Molnar, P., 1980. Microearthquake seismicity and fault plane solutions in the Hindu Kush region and their tectonic implications. *Journal of Geophysical Research 85*, 1365-1387.

DeCelles, P. G., Robinson, D. M., & Zandt, G., 2002. Implications of shortening in the Himalayan fold-thrust belt for uplift of the Tibetan Plateau. *Tectonics*, *21*(6), 1062, doi:10.1029/2001TC001322.

Duretz, T., Gerya, T. V., & May, D. A., 2011. Numerical modelling of spontaneous slab breakoff and subsequent topographic response. *Tectonophysics*, *502*(1), 244-256.

Duretz, T., Schmalholz, S. M., & Gerya, T. V., 2012. Dynamics of slab detachment. *Geochemistry, Geophysics, Geosystems*, *13*(3), doi: 10.1029/2011GC004024.

Engdahl, E. R., van der Hilst, R., & Buland, R., 1998. Global teleseismic earthquake relocation with improved travel times and procedures for depth determination. *Bulletin of the Seismological Society of America*, *88*(3), 722-743.

Feld, C., Haberland, C., Schurr, B., Sippl, C., Wetzel, H. U., Roessner, S., Ickrath, M., Abdybachaev, U., & Orunbaev, S., 2015. Seismotectonic study of the Fergana Region (Southern Kyrgyzstan): distribution and kinematics of local seismicity. *Earth, Planets and Space*, *67*(1), 1-13.

GEOFON Data Centre, 1993. GEOFON Seismic Network. Deutsches GeoForschungsZentrum GFZ. Other/Seismic Network. doi:10.14470/TR560404.

Guillot, S., Garzanti, E., Baratoux, D., Marquer, D., Mahéo, G., & De Sigoyer, J., 2003. Reconstructing the total shortening history of the NW Himalaya. *Geochemistry, Geophysics, Geosystems*, *4*(7), 1064, doi:10.1029/2002GC000484.

Hardebeck, J. L., & Shearer, P. M., 2002. A new method for determining first-motion focal mechanisms. *Bulletin of the Seismological Society of America*, *92*(6), 2264-2276.

Institute of Seismology, National Academy of Sciences of Kyrgyz Republic (KIS), 2007. Kyrgyz Digital Network. International Federation of Digital Seismograph Networks. Other/Seismic Network. doi:10.7914/SN/KR.

ISC bulletins, International Seismological Centre, 2013. *On-line Bulletin*, http://www.isc.ac.uk, Internatl. Seis. Cent., Thatcham, United Kingdom.

Kennett, B. L. N., Engdahl, E. R., & Buland, R., 1995. Constraints on seismic velocities in the Earth from travel times. *Geophysical Journal International*, *122*(1), 108-124.

Kind, R., & Yuan, X., 2010. Seismic images of the biggest crash on Earth. *Science*, *329*(5998), 1479-1480.

KNDC/Institute of Geophysical Research (Kazakhstan), 1994. Kazakhstan Network. International Federation of Digital Seismograph Networks. Other/Seismic Network. doi:10.7914/SN/KZ.

Koulakov, I., 2009. LOTOS code for local earthquake tomographic inversion: benchmarks for testing tomographic algorithms. *Bulletin of the Seismological Society of America*, *99*(1), 194-214.

Koulakov, I., & Sobolev, S. V., 2006. A tomographic image of Indian lithosphere break-off beneath the Pamir–Hindukush region. *Geophysical Journal International*, *164*(2), 425-440.

Krieger, L. & Heimann, S., 2012. MoPaD; moment tensor plotting and decomposition; a tool for graphical and numerical analysis of seismic moment tensors. *Seismological Research Letters*, 83(3):589-595.

Kumar, M. R., Saul, J., Sarkar, D., Kind, R., & Shukla, A. K., 2001. Crustal structure of the Indian shield: New constraints from teleseismic receiver functions. *Geophysical Research Letters*, *28*(7), 1339-1342.

Laske, G. Masters., G., Ma, Z., Pasyanos, M., 2013. Update on CRUST1.0 - A 1-degree Global Model of Earth's Crust. In *Geophys. Res. Abstracts* (Vol. 15). Abstract EGU2013-2658.

Li, C., Van der Hilst, R. D., Meltzer, A. S., & Engdahl, E. R., 2008. Subduction of the Indian lithosphere beneath the Tibetan Plateau and Burma. *Earth and Planetary Science Letters*, *274*(1), 157-168.

Lister, G., Kennett, B., Richards, S., & Forster, M., 2008. Boudinage of a stretching slablet implicated in earthquakes beneath the Hindu Kush. *Nature Geoscience*, *1*(3), 196-201.

Lomax, A., Virieux, J., Volant, P., & Berge-Thierry, C., 2000. Probabilistic earthquake location in

3D and layered models. In *Advances in seismic event location* (pp. 101-134). Springer Netherlands.

Magni, V., Hunen, J. V., Funiciello, F., & Faccenna, C., 2012. Numerical models of slab migration in continental collision zones. *Solid Earth*, *3*(2), 293-306.

Mechie, J., Yuan, X., Schurr, B., Schneider, F., Sippl, C., Ratschbacher, L., Minaev, V., Gadoev, M., Oimahmadov, I., Abdybachaev, U., Moldobekov, B., Orunbaev, S., & Negmatullaev, S., 2012. Crustal and uppermost mantle velocity structure along a profile across the Pamir and southern Tien Shan as derived from project TIPAGE wide-angle seismic data. *Geophysical Journal International*, *188*(2), 385-407.

Michael, A. J., 1987. Use of focal mechanisms to determine stress: a control study. *Journal of Geophysical Research*, *92*, 357-368.

Mitra, S., Priestley, K., Gaur, V. K., Rai, S. S., & Haines, J., 2006. Variation of Rayleigh wave group velocity dispersion and seismic heterogeneity of the Indian crust and uppermost mantle. *Geophysical Journal International*, *164*(1), 88-98.

Molnar, P., & Stock, J. M., 2009. Slowing of India's convergence with Eurasia since 20 Ma and its implications for Tibetan mantle dynamics. *Tectonics*, *28*(3), doi: 10.1029/2008TC002271.

Nábělek, J., Hetényi, G., Vergne, J., Sapkota, S., Kafle, B., Jiang, M., Su, H., Chen, J., & Huang, B. S., 2009. Underplating in the Himalaya-Tibet collision zone revealed by the Hi-CLIMB experiment. *Science*, *325*, 1371-1374.

Negredo, A. M., Replumaz, A., Villaseñor, A., & Guillot, S., 2007. Modeling the evolution of continental subduction processes in the Pamir–Hindu Kush region. *Earth and Planetary Science Letters*, *259*(1), 212-225.

Paige, C. C., & Saunders, M. A., 1982. LSQR: An algorithm for sparse linear equations and sparse least squares. *ACM Transactions on Mathematical Software (TOMS)*, *8*(1), 43-71.

Pegler, G., & Das, S., 1998. An enhanced image of the Pamir–Hindu Kush seismic zone from relocated earthquake hypocentres. *Geophysical Journal International*, *134*(2), 573-595.

PMP International (Tajikistan), 2005. Tajikistan National Seismic Network. International Federation of Digital Seismograph Networks. Other/Seismic Network. doi:10.7914/SN/TJ.

Replumaz, A., Negredo, A. M., Guillot, S., & Villaseñor, A., 2010. Multiple episodes of continental subduction during India/Asia convergence: Insight from seismic tomography and tectonic recon-struction. *Tectonophysics*, *483*(1), 125-134.

Roecker, S. W., 1982. Velocity structure of the Pamir-Hindu Kush Region: Possible evidence of subducted crust. *Journal of Geophysical Research*, *87*, 945-959.

Schmidt, J., Hacker, B. R., Ratschbacher, L., Stübner, K., Stearns, M., Kylander-Clark, A., Cottle, J. M., Webb, A. A. G., Gehrels, G., & Minaev, V., 2011. Cenozoic deep crust in the Pamir. *Earth and Planetary Science Letters*, *312*, 411-421.

Schneider, F. M., Yuan, X., Schurr, B., Mechie, J., Sippl, C., Haberland, C., Minaev, V., Oimahmadov, I., Gadoev, M., Radjabov, N., Abdybachaev, U., Orunbaev, S., & Negmatullaev, S., 2013. Seismic imaging of subducting continental lower crust beneath the Pamir. *Earth and Planetary Science Letters*, *375*, 101-112.

Schneider, F. M., 2014. Imaging an Intra-continental Subduction in Central Asia with Teleseismic Receiver Functions. *Scientific Technical Report* 14/6*, Deutsches GeoForschungsZentrum GFZ***,** Potsdam, 179 p, doi:10.2312/GFZ.b103-14063.

Schurr, B., & Nábělek, J., 1999. New techniques for the analysis of earthquake sources from local array data with an application to the 1993 Scotts Mills, Oregon, aftershock sequence. *Geophysical Journal International*, *137*(3), 585-600.

Schurr, B., Yuan, X., Haberland, C., Kufner, S.-K., 2012: TIPTIMON (Tien Shan-Pamir Monitoring Program) TAJIKISTAN (2012/2014). Deutsches GeoForschungsZentrum GFZ. Other/Seismic Network. doi: 10.14470/0P7567352807.

Schurr, B., Yuan, X., Haberland, C., Kufner, S.-K., 2013: TIPTIMON (Tien Shan-Pamir Monitoring Program) AFGHANISTAN (2013/2014). Deutsches GeoForschungsZentrum GFZ. Other/Seismic Network. doi: 10.14470/1P7568352842.

Schwab, M., Ratschbacher, L., Siebel, W., McWilliams, M., Minaev, V., Lutkov, V., Chen, F., Stanek, K., Nelson, B., Frisch, W., & Wooden, J. L., 2004. Assembly of the Pamirs: Age and origin of magmatic belts from the southern Tien Shan to the southern Pamirs and their relation to Tibet. *Tectonics*, *23*(4), TC4002, doi: 10.1029/2003TC001583.

Scripps Institution of Oceanography, 1986. IRIS/IDA Seismic Network. International Federation of Digital Seismograph Networks. Other/Seismic Network. doi:10.7914/SN/II.

Sippl, C., Schurr, B., Yuan, X., Mechie, J., Schneider, F. M., Gadoev, M., Orunbaev, S., Oimahmadov, I., Haberland, C., Abdybachaev, U., Minaev, V., Negmatullaev, S., & Radjabov, N., 2013a. Geometry of the Pamir-Hindu Kush intermediate-depth earthquake zone from local seismic data. *Journal of Geophysical Research: Solid Earth*, *118*(4), 1438-1457.

Sippl, C., Schurr, B., Tympel, J., Angiboust, S., Mechie, J., Yuan, X., Schneider, F. M., Sobolev, S. V., Ratschbacher, L., & Haberland, C., 2013b. Deep burial of Asian continental crust beneath the Pamir imaged with local earthquake tomography. *Earth and Planetary Science Letters*, *384*, 165-177.

Smit, M. A., Ratschbacher, L., Kooijman, E., & Stearns, M. A., 2014. Early evolution of the Pamir deep crust from Lu-Hf and U-Pb geochronology and garnet thermometry. *Geology*, *42*(12), 1047-1050.

Sobolev, S. V., Zeyen, H., Granet, M., Achauer, U., Bauer, C., Werling, F., Altherr, R. & Fuchs, K., 1997. Upper mantle temperatures and lithosphere-asthenosphere system beneath the French Massif Central constrained by seismic, gravity, petrologic and thermal observations. *Tectonophysics*, *275*(1), 143-164.

34

Stearns, M. A., Hacker, B. R., Ratschbacher, L., Lee, J., Cottle, J. M., & Kylander-Clark, A., 2013. Synchronous Oligocene–Miocene metamorphism of the Pamir and the north Himalaya driven by plate-scale dynamics. *Geology*, *41*(10), 1071-1074.

Stearns, M.A., Hacker, B.R., Ratschbacher, L., Rutte, D., Kylander-Clark, A.R.C., 2015. Titanite petrochronology of the Pamir gneiss domes: Implications for mid–deep crust exhumation and titanite closure to Pb and Zr diffusion. *Tectonics*, 34, 784-802, doi: 10.1002/ 2014TC003774.

Stübner, K., Ratschbacher, L., Rutte, D., Stanek, K., Minaev, V., Wiesinger, M., Gloaguen, R., & Project TIPAGE members, 2013. The giant Shakhdara migmatitic gneiss dome, Pamir, India-Asia collision zone: 1. Geometry and kinematics. *Tectonics*, *32*(4), 948-979.

Tapponnier, P., Mattauer, M., Proust, F., & Cassaigneau, C., 1981. Mesozoic ophiolites, sutures, and large-scale tectonic movements in Afghanistan. *Earth and Planetary Science Letters*, *52*(2), 355-371.

Treloar, P. J., & Izatt, C. N., 1993. Tectonics of the Himalayan collision between the Indian Plate and the Afghan Block: a synthesis. *Geological Society, London, Special Publications*, *74*(1), 69-87.

USGS earthquake bulletins, 2015. *On-line Bulletin*, http://earthquake.usgs.gov/, United States Geological Survey, USA.

Van der Voo, R., Spakman, W., & Bijwaard, H., 1999. Tethyan subducted slabs under India. *Earth and Planetary Science Letters*, *171*(1), 7-20.

Van Hinsbergen, D. J., Kapp, P., Dupont-Nivet, G., Lippert, P. C., DeCelles, P. G., & Torsvik, T. H., 2011. Restoration of Cenozoic deformation in Asia and the size of Greater India. *Tectonics*, *30*(5), doi: 10.1029/2011TC002908.

Vinnik, L. P., Lukk, A. A., & Nersesov, I. L., 1977. Nature of the intermediate seismic zone in the mantle of Pamirs-Hindu-Kush. *Tectonophysics*, *38*(3), T9-T14.

Waldhauser, F., & Ellsworth, W. L., 2000. A double-difference earthquake location algorithm: Method and application to the northern Hayward fault, California. *Bulletin of the Seismological Society of America*, *90*(6), 1353-1368.